npj | Flexible Electronics

www.nature.com/npjflexelectron

ARTICLE OPEN

Check for updates

Elastic organic crystals with ultralong phosphorescence for flexible anti-counterfeiting

Kaiwei Huang[1], Lulu Song[1], Kun Liu[1], Anqi Lv[1], Manjeet Singh[1], Kang Shen[1], Jing Shen[1], Jiamin Wang[1], Hongchen Wang[1], Huifang Shi[1], Huili Ma[1], Mingxing Gu[1], Gengzhi Sun[1], Wei Yao[1]✉, Zhongfu An[1]✉ and Wei Huang[1,2]✉

Ultralong organic phosphorescence (UOP) crystals have attracted increased attention due to the distinct photophysical property of a long-lived lifetime. However, organic crystals are generally brittle, leading to a serious problem for their application in flexible technology. Herein, we report three types of elastic organic crystals (EOCs) with ultralong phosphorescence via introducing halogen atoms (Cl, Br, I) into π-conjugated phosphorescent molecules. Especially, the crystal containing iodine atoms displayed both excellent elasticity ($\varepsilon = 3.01\%$) and high phosphorescent efficiency ($\Phi_{Ph} = 19.1\%$) owing to the strong halogen bonds. Taking advantage of its highly efficient UOP and excellent elasticity, we successfully used a DCz4I crystal for anti-counterfeiting application. These findings may provide guidance for the development of elastic crystals with afterglow and expand the scope of potential applications on flexible materials.

npj Flexible Electronics (2021)5:21 ; https://doi.org/10.1038/s41528-021-00117-9

INTRODUCTION

Flexible electronics is becoming an emerging research field with a rapid growth rate due to their innovative applications in displays[1,2], electronic skin[3], and solar cells[4], which accelerate the course of flexible materials. To date, such many flexible materials including metals[5], inorganic materials[6], 2D-materials[7], organics[8–10], and so forth, have been developed. Thereinto, organics show great promise in high-performance device applications owing to their extensive resource, tunable functions, and well processability. Flexible organic materials contain polymers[10–12], liquid crystals[13,14], and organic crystals[15–19]. Organic crystals especially display excellent performances owing to their ordered molecular packing. However, weak intermolecular interactions usually result in the rigidity and fragility of organic crystals[20]. Elastic organic crystals (EOCs) have been realized recently via π···π stacking and multi-directional halogen or hydrogen bonds[21–23]. The luminescent properties of EOCs play an important role in the applications of flexible devices. To date, series of EOCs with short-lived luminescence (≤1 ms) have been developed[24–27]. However, there still is no report on the flexible crystals with afterglow feature (>100 ms), although afterglow materials show superiority in optoelectronic with long-lived lifetimes[25].

Ultralong organic phosphorescence (UOP) has attracted increased attention due to long-lived lifetimes and rich excited state properties[28,29]. Different from inorganic and organometallic phosphors[30], purely organic luminescent materials with UOP features at room temperature are rare owing to the forbidden singlet-to-triplet transition and fast non-radiative decay of the excitons. Many rational strategies have been used to obtain efficient phosphorescence, for example, the introduction of carbonyl or halogen atoms to promote the intersystem crossing (ISC) and the construction of a rigid environment to suppress the non-radiative transitions[31,32]. To construct rigid environments, researchers have proposed several methods, including crystallization[33–37], host–guest doping methods[38–40], self-assembly[41,42], and so on[43–45]. Crystal engineering is an indispensable method to reduce non-radiative decay by efficiently restricting molecular motions. Inspired by the requirement of the reversible deformation of crystals and efficient UOP, we reasoned that halogen atoms and π-conjugated phosphorescent chromophores will be suitable candidates as molecular structural units to construct elastic crystals (Fig. 1a). Meanwhile, the high phosphorescence efficiency can be achieved by introducing the halogen atoms to increase ISC (Fig. 1b).

RESULTS AND DISCUSSION

Construction of EOCs with ultralong phosphorescence

To validate our hypothesis, we designed and synthesized a series of molecules, namely, 9,9′-(6-(4-chlorophenoxy)-1,3,5-triazine-2,4-diyl)bis(9H-carbazole) (DCz4Cl), 9,9′-(6-(4-bromophenoxy)-1,3,5-triazine-2,4-diyl)bis(9H-carbazole) (DCz4Br), and 9,9′-(6-(4-Iodophenoxy)-1,3,5-triazine-2,4-diyl)bis(9H-carbazole) (DCz4I) (Fig. 1c) via two-step reaction as shown in Supplementary Fig. 1. Their chemical structures were characterized by NMR spectroscopy (see Supplementary Figs. 2–7) and single crystal analysis. The purity of the target compounds was verified by high-performance liquid chromatography (HPLC) (See Supplementary Fig. 8) and elemental analysis (see Methods for more details). After slow evaporation in a mixture of dichloromethane and ethanol at room temperature, acicular crystals (length of 10–15 mm) of these three molecules are formed. Figure 1d displays fluorescence and afterglow microscopy images of these crystals, demonstrating that the obtained crystals have excellent elasticity and UOP characteristics. These crystals were subject to a manually mechanical test to assess their bending response. One end of the individual crystal was fixed with silicone grease, while the other end was pushed under stress with a pin (See Supplementary Figs. 9–11). All crystals bent into semicircle under mechanical stress without breakage and quickly regained its initial straight shape upon withdrawal of

[1]Key Laboratory of Flexible Electronics (KLOFE) & Institute of Advanced Materials (IAM), Nanjing Tech University (NanjingTech), Nanjing, People's Republic of China. [2]Frontiers Science Center for Flexible Electronics (FSCFE), Shaanxi Institute of Flexible Electronics (SIFE) & Shaanxi Institute of Biomedical Materials and Engineering (SIBME), Northwestern Polytechnical University (NPU), Xi'an, China. ✉email: iamwyao@njtech.edu.cn; iamzfan@njtech.edu.cn; iamwhuang@nwpu.edu.cn

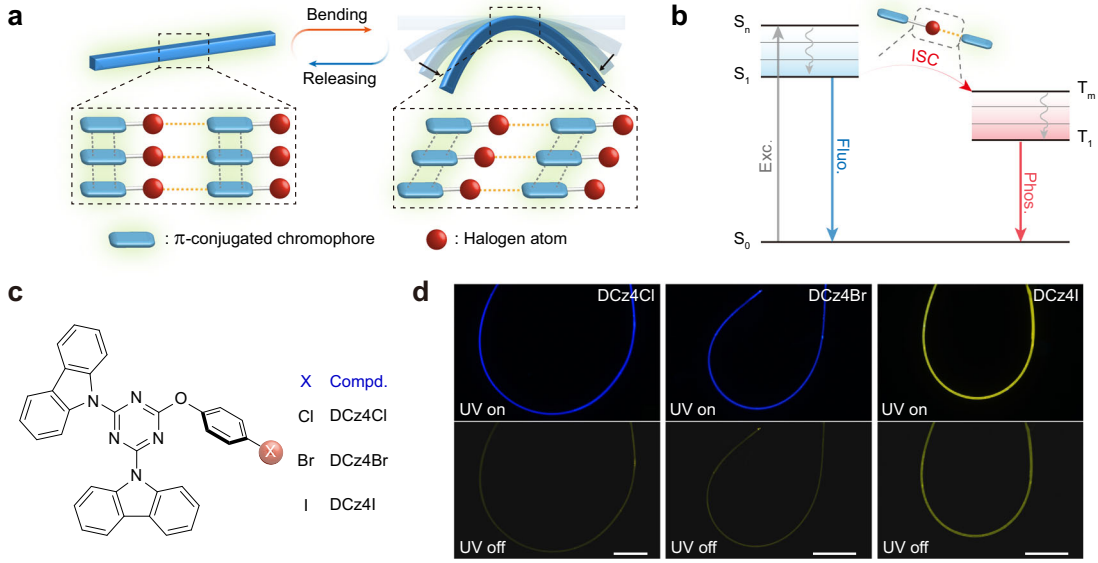

Fig. 1 Schematic illustration of the elastic organic crystals with ultralong phosphorescence. a Design concept for elastic organic crystals. **b** Proposed mechanism of highly efficient ultralong organic phosphorescence. **c** Chemical structures of target molecules. **d** The fluorescence microscopy images of curving crystals from target molecules under UV on and off, the scale bars are 500 μm.

pressure. The reversible bending-relaxation phenomenon of all the crystals can be cycled many times (See Supplementary Movies 1–3), demonstrating the fatigueless and restorative character of these crystals. Elastic strains (ε) of these crystals were estimated by the equation $\varepsilon = t/2\,R$, where R is the radius of curvature and t is the thickness of the crystal (See Supplementary Fig. 12 and Supplementary Table 1). The obtained ε values for DCz4Cl, DCz4Br, and DCz4I crystals are 3.99, 3.42, and 3.01%, respectively. The ε of these three crystals are higher than most of the reported EOCs ($\varepsilon < 3\%$)[46,47]. Compared with the fluorescence microscopy images of crystals at straight state in Supplementary Fig. 13, the luminescence of crystals displayed no difference when they deformed into semicircle shape. As shown in Fig. 1d, the crystals of DCz4Cl and DCz4Br exhibited blue emission under UV light and weak yellow persistent luminescence after removing UV irradiation (See Supplementary Movies 4 and 5). Impressively, bright yellow emission can be observed from the DCz4I crystal before and after turning off irradiation (See Supplementary Movie 6), indicating that DCz4I may have high phosphorescence quantum efficiency (QE).

UOP and elasticity characterization of obtained EOCs

Firstly, we investigated the photophysical properties of these phosphors in both solution and crystal states. The profiles of absorption and photoluminescence spectra for these phosphors in the dilute tetrahydrofuran solution (1×10^{-5} mol L^{-1}) were similar, revealing that the halogen substituents didn't influence the emission in the single-molecule state (See Supplementary Figs. 14–16). In the crystalline state, on 350 nm irradiation, these molecules have an intense fluorescent band in the range of 360 to 450 nm (Fig. 2a). Obvious phosphorescent emission peaks, after a delay time of 8 ms, appear around 530 nm with ultralong lifetimes of 526 ms for DCz4Cl, 307 ms for DCz4Br, and 268 ms for DCz4I (Fig. 2b, Supplementary Figs. 17–22, and Supplementary Tables 2–3). The exponential decay in the logarithmic plot of the emission decay profile (See Supplementary Fig. 23) further confirmed that the emission with long-lived lifetimes of these crystals were originated from phosphorescence[48]. It is worth noting that the lifetimes of these three crystals became shorter after bending due to the change of the molecular packing mode (See Supplementary Fig. 24 and Supplementary Table 4). As the atomic mass of halogen substituents increases from Cl to I, the phosphorescence QE is enhanced gradually. It's worth noting that Φ_{Ph} of DCz4I reached as high as 19.1%, 34 times over that of DCz4Cl (0.54%) (Fig. 2c). Excitation-phosphorescence mapping for DCz4Cl and DCz4Br crystals exhibited an obviously delayed fluorescence emission (Fig. 2d and Supplementary Fig. 25). The DCz4I phosphor has an intense and individual emission in crystal, belonging to phosphorescence, from 500 to 650 nm without emission peaks for delayed fluorescence (Fig. 2e). This comparison indicated that the iodine atom can effectively promote the ISC and boost triplet excitons. To uncover the high phosphorescence efficiency of DCz4I in crystal, the single crystal analysis, photophysical parameter calculations, and theoretical simulations were conducted. As shown in Fig. 3a, DCz4I crystal has dual C–I···π interactions with 3.547 and 3.571 Å distance. In contrast, there is only one bonding interaction between halogen atoms and adjacent molecules in DCz4Cl and DCz4Br crystals. Furthermore, the binding energy of C–I···π bonding in a DCz4I dimer, calculated by Gaussian 09, is 37.69 KJ/mol, larger than that of C–H···Cl (12.43 KJ mol^{-1}) and C–H···Br (20.43 KJ mol^{-1}) (Fig. 3b). The high binding energy in DCz4I dimer promotes its heavy-atom effect for boosting triplet excitons. According to the formula derived in supporting information, the rate of intersystem crossing (k_{ISC}) and radiative decay ($k_{r,P}$) can be calculated from fluorescence quantum yields, Φ_{Ph}, and emission lifetimes (See Supplementary Table 5). It was found that the k_{ISC} and $k_{r,P}$ for DCz4I crystal are faster than that of DCz4Cl and DCz4Br (Fig. 3c). As anticipated, the calculated SOC constants ξ (S_1, T_2) in the dimer of DCz4I (3.099 cm^{-1}) is larger than that of DCz4Cl (0.033 cm^{-1}) and DCz4Br (0.199 cm^{-1}) (See Supplementary Figs. 26, 27). For DCz4I crystals, the smaller recombination energy means that there is a smaller structural change in the relaxation process of the excited state and non-radiative deactivation (See Supplementary Fig. 28). Taken the strong heavy-atom effect, k_{ISC}, ξ, and reorganization energy, DCz4I have an effective ISC, which is consistent with high phosphorescence QE.

We calculated the attachment energy of these crystals by Materials Studio 7.0 to ensure the molecular arrangements of crystals. The maximum attachment energy in DCz4I crystal is (200) face, indicating that the length direction of crystal is along a axis (See Supplementary Fig. 29 and Supplementary Tables 7–9). The bending process occurs on (011) plane which were the widest faces of the crystal perpendicular to the a axis. As shown in Fig. 3d,

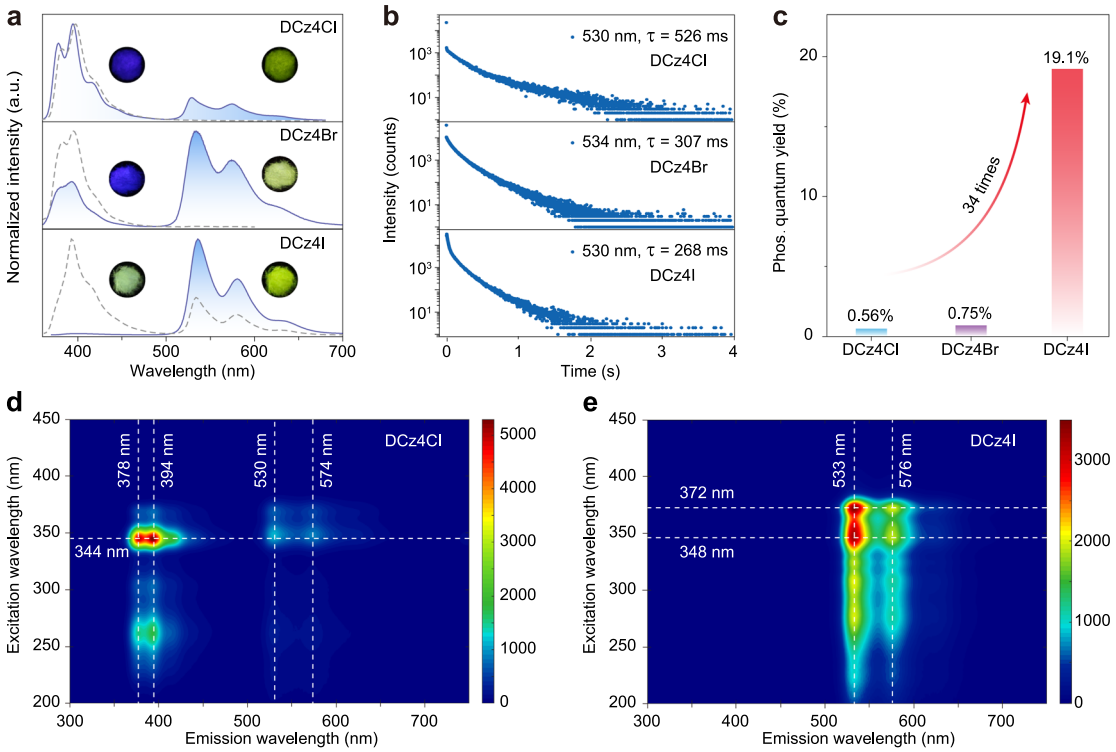

Fig. 2 Photophysical properties of DCz4Cl, DCz4Br, and DCz4I in the crystalline state under ambient conditions (298 K). a Steady-state photoluminescence (gray dashed lines) and phosphorescence spectra (blue solid lines). **b** Lifetime decay profiles of the ultralong phosphorescence bands excited by optimum excitation wavelength. **c** The histogram of phosphorescence quantum yield. **d** Excitation-phosphorescence emission mapping of DCz4Cl crystals. **e** Excitation-phosphorescence emission mapping of DCz4I crystals.

in this direction, the π···π interactions with a vertical distance of 3.493 Å construct molecular chains. In these molecular chains, the distances between molecular units were enlarged during the expansion process and compressed in the contraction process (See Supplementary Fig. 30)[22], leading to the increases of non-radiative and decreases of lifetimes. The intermolecular C–H···π (2.881 and 2.893 Å) and C–I···π (3.547 and 3.571 Å) interactions have bonded the adjacent molecules between the molecular layers during the bending and releasing process (Fig. 3d), which can facilitate crystals return to their original state. A DCz4I molecule is connected with four neighbor ones by multi-directional and numerous intermolecular C–H···π, C–I···π, and C–H···O interactions along the crystallographic planes (Fig. 3e). These weak interactions act as a buffer for the bending of the crystal, preventing crystals from breaking[46]. With similar molecular arrangements and interactions (See Supplementary Figs. 31–33), DCz4Cl and DCz4Br crystals all showed excellent elasticity. Our results demonstrate the impact of π···π stacking and halogen bonds on elasticity in crystals, providing guidance for the development of flexible crystals.

Anti-counterfeiting of flexible banknotes

On the basis of the high UOP efficiency and ultralong emission lifetimes of these elastic crystals, we further successfully demonstrated their potential in an anti-counterfeiting application for a flexible banknote. As demonstrated in Fig. 4a, the DCz4I crystal with high phosphorescent efficiency and elasticity has embedded beneath the letters "IAM" on a model banknote. The whole banknote emitted strong blue fluorescence under the irradiation of the UV lamp (365 nm). Bright yellow afterglow, emitting from the crystal, penetrated through the banknotes after turning off the irradiation (Fig. 4b). As the banknote bent under the applied force, the crystal deformed along with it. A curved crystal with intense persistent luminescence in banknote can last several seconds after switching off the UV lamp (Fig. 4c). Moreover, the micron wire can maintain its mechanical properties and phosphorescent properties after being bent many times. (See Supplementary Fig. 34) This unique elastic organic crystal with strong and long afterglow cannot be easily counterfeited, for the complete crystal in the banknote can be checked under the microscope. This showed the great prospect of elastic crystals with UOP in the practical application of banknote anti-counterfeiting.

In summary, we have developed a series of EOCs with UOP through a valid design principle by adjusting halogen atoms. Crystals DCz4Cl, DCz4Br, and DCz4I show outstanding elasticity with elastic strains over 3%. Among them, DCz4I crystals demonstrated high phosphorescence QE (19.1%) under ambient conditions. Combing theoretical simulations and single crystal analysis, we speculated that infinite π···π stacking and halogen/C–H···X bonds between molecular layers sever as critical factors for the highly elastic deformation of crystals. Given the perfect combination of flexibility and afterglow feature, the crystal was applied to anti-counterfeiting of flexible banknotes. We believe that the present work will be a huge step forward in the development of flexible electronics and applications incorporating such elastic UOP molecular systems.

METHODS

Reagents and materials

Unless noted, all reagents used in the experiments were purchased from commercial sources without further purification.

Measurements

Nuclear magnetic resonance (^{1}H and ^{13}C NMR) spectra were collected using Mercury-Vx-300 M Nuclear Magnetic Resonance. The chemical shift was relative to tetramethylsilane (TMS) as the internal standard. Resonance patterns were reported with the notation s (singlet), d (doublet), t (triplet),

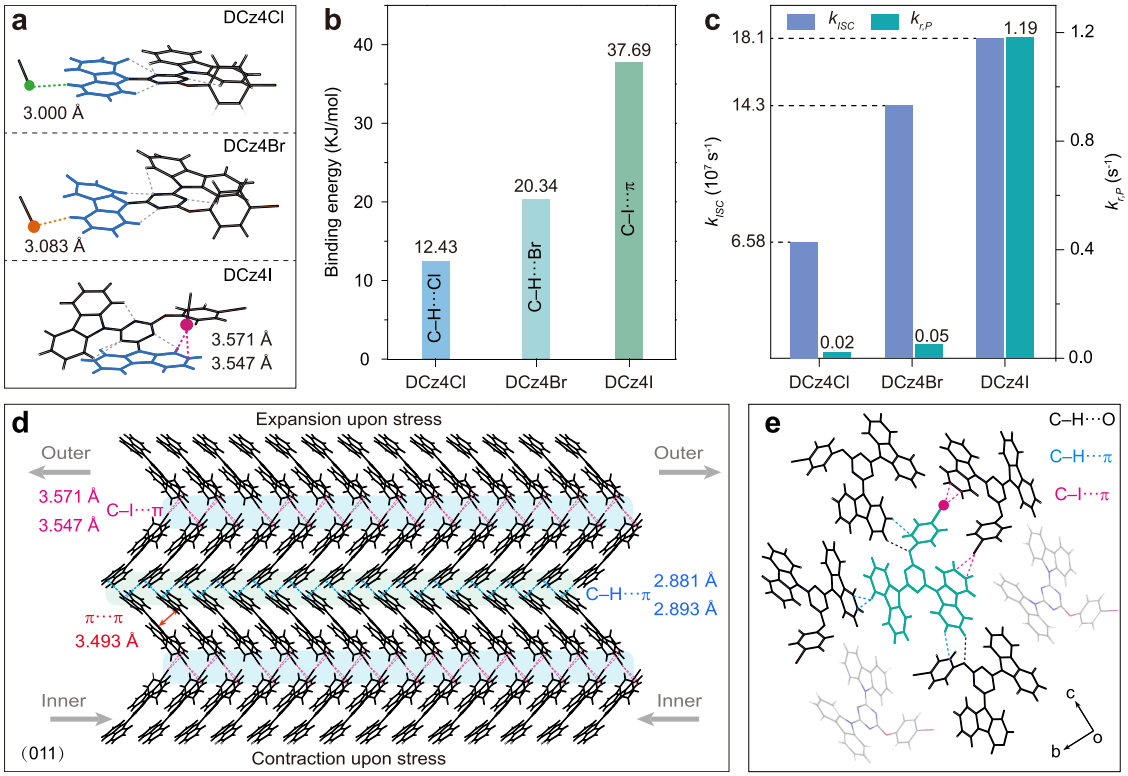

Fig. 3 Mechanism investigation on the elastic organic crystals with ultralong phosphorescence under ambient conditions. a Interactions between halogen atoms and adjacent molecules in DCz4Cl, DCz4Br, and DCz4I crystals. Gray dashed lines represent C–H···N hydrogen bonds. Green, orange, and violet dashed lines represent C–H···Cl, C–H···Br, and C–I···π bonding, respectively. **b** The absolute value of binding energy in DCz4Cl, DCz4Br, and DCz4I dimers calculated at the level of B3LYP/6-31+G*. **c** $k_{r,P}$ and k_{ISC} of DCz4Cl, DCz4Br, and DCz4I in the crystalline state under ambient conditions (298 K). **d** Molecular packing of DCz4I crystal viewed down the (011) plane. **e** Multiple intermolecular interactions (marked by a broken line) between one molecule and four neighboring ones.

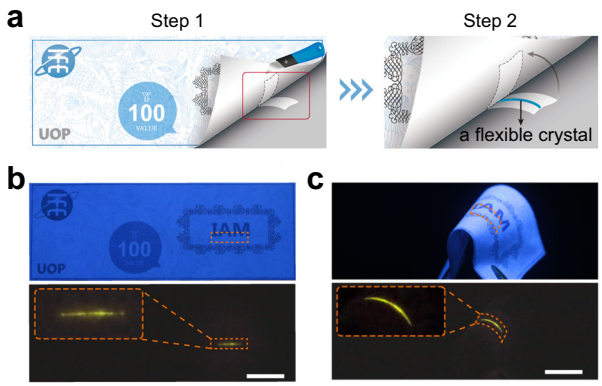

Fig. 4 Demonstration of elastic crystals with highly efficient UOP for anti-counterfeit application of flexible banknotes. a The preparation process of anti-counterfeiting. A crystal of DCz4I was embedded into the banknote. **b** Photographs taken under UV on and off. **c** Photographs taken under UV on and off when the banknote was bent, the scale bars are 1.5 cm.

q (quartet), and m (multiplet). Gel filtration chromatography was performed using a Sun Fire TM C18 column conjugated to an ACQUITY UPLCH-class water HPLC system. Before running, each sample was purified via a 0.22 μm filter to remove any aggregates. The flow rate was fixed at 1.0 mL min^{-1}, the injection volume was 1 μL, and each sample was run for 10 min. Tensile tests were carried out on the HY-0350 micro-control electronic material testing machine. Elemental analysis was characterized by instruments Germany Vario EL cube. UV-visible absorption spectra were measured by Shimadzu UV-1750. Steady-state photoluminescence, excitation, and phosphorescence spectra were measured using Hitachi F-4600 under ambient conditions. The lifetimes and time-resolved emission spectra of numerous crystals were obtained on Edinburgh FLSP920 fluorescence spectrophotometer equipped with a xenon arc lamp (Xe900), a nanosecond hydrogen flash-lamp (nF920), and a microsecond flash-lamp (μF900), respectively. To measure the lifetimes of a single crystal, the crystal was excited locally with a 360 nm LD pumped all-solid-state UV laser (Changchun New Industries Optoelectronics Tech, UV-FN-360, 50 mW) focused down to the diffraction limit. The excitation laser was filtered with a 400 nm notch filter. The light was subsequently coupled to a grating spectrometer (Andor, KY328i-B2) and recorded by a thermal-electrically cooled time-resolved CCD (Andor, DH334T-18U-03) with a delay time of 2 ms. Photoluminescence QE was collected on a Hamamatsu Absolute PL Quantum Yield Spectrometer C11347 under ambient conditions. X-ray crystallography was achieved using a Bruker SMART APEX-II CCD diffractometer with graphite monochromated Mo-Kα radiation at 293 K. Exposure time is 11 s and test time is about 2 h. The luminescent photos of stacked crystals were taken by a Canon EOS 700 D camera under ambient conditions. Fluorescence and afterglow images of one crystal were recorded using a Nikon DS-Ri2 Microscope Camera. The excitation source is a mercury lamp (Nikon INTENSILIGHT C-HGFI) equipped with a band-pass filter (330–380 nm for UV light).

The preparation of crystals

Needle-like crystals of these three molecules were prepared by slow evaporation in a mixture of dichloromethane and ethanol in a ratio of 4:1 at room temperature.

Computational details

For model systems, the DCz4Cl, DCz4Br, and DCz4I molecules were extracted from the crystal structure. The optimization of the T_1 state was used B3LYP functional with mix basis set, DEF2-SVP basis set was used for H, C, N, and O atoms while LANL2DZ basis set for I atom. In the case of the

dimer, the interaction between halogens and carbazole of a contiguous molecule was observed. We then turned to look at the low-lying excited state structure of dimer, including excitation energies and natural transition orbitals (NTOs) with a Time-Dependent Density Functional Theory (TD-DFT) approach. DEF2-TZVP basis set was used for H, C, N, and O atoms while X2C-TZVP all basis set for I atom at B3LYP/GEN level. The mixed basis set can be used with the GEN keyword. At the same level, the spin–orbit coupling (SOC) constants (ξ) of molecules between singlet and triplet states were given by Beijing Density Function (BDF) program. The binding energy was calculated using B3LYP with 6–31+G* basis sets used for H, C, N, and O atoms while SDD basis set for I atom at B3LYP/GEN level, respectively. The reorganization energy was calculated using B3LYP with 6–31+G* basis sets used for H, C, N, and O atoms while SDD basis was set for halogen atom at B3LYP/def2SVP level. The above results are calculated by Gaussian 09 package.

DATA AVAILABILITY

The data that support the findings of this study are available from the authors on reasonable request.

Received: 15 January 2021; Accepted: 5 July 2021;
Published online: 16 August 2021

REFERENCES

1. Hosseini, P., Wright, C. D. & Bhaskaran, H. An optoelectronic framework enabled by low-dimensional phase-change films. *Nature* **511**, 206–211 (2014).
2. Choi, S. et al. Multi-directionally wrinkle-able textile OLEDs for clothing-type displays.*npj Flex. Electron.* **4**, 33 (2020).
3. Núñez, C. G., Manjakkal, L. & Dahiya, R. Energy autonomous electronic skin. *npj Flex. Electron.* **3**, 1 (2019).
4. Gao, L. et al. Flexible, transparent nanocellulose paper-based perovskite solar cells. *npj Flex. Electron.* **3**, 4 (2019).
5. Chauvin, A. et al. Vapor dealloying of ultra-thin films: a promising concept for the fabrication of highly flexible transparent conductive metal nanomesh electrodes. *npj Flex. Electron.* **3**, 5 (2019).
6. Linghu, C., Zhang, S., Wang, C. & Song, J. Transfer printing techniques for flexible and stretchable inorganic electronics. *npj Flex. Electron.* **2**, 26 (2018).
7. Datta, R. S. et al. Flexible two-dimensional indium tin oxide fabricated using a liquid metal printing technique. *Nat. Electron.* **3**, 51–58 (2020).
8. Zabihipour, M. et al. High yield manufacturing of fully screen-printed organic electrochemical transistors. *npj Flex. Electron.* **4**, 15 (2020).
9. Oh, J. Y. et al. Intrinsically stretchable and healable semiconducting polymer for organic transistors. *Nature* **539**, 411–415 (2016).
10. Wei, C. et al. Organic Janus microspheres: a general approach to all-color dual-wavelength microlasers. *J. Am. Chem. Soc.* **141**, 5116–5120 (2019).
11. Rozyyev, V. et al. High-capacity methane storage in flexible alkane-linked porous aromatic network polymers. *Nat. Energy* **4**, 604–611 (2019).
12. Bergqvist, J. et al. Asymmetric photocurrent extraction in semitransparent laminated flexible organic solar cells. *npj Flex. Electron.* **2**, 4 (2018).
13. Xu, F. F. et al. Flat-panel laser displays based on liquid crystal microlaser arrays. *CCS Chem.* **2**, 369–375 (2020).
14. Zhang, C. et al. A contact-sliding-triboelectrification-driven dynamic optical transmittance modulator for self-powered information covering and selective visualization. *Adv. Mater.* **32**, 1904988 (2020).
15. Owczarek, M. et al. Flexible ferroelectric organic crystals. *Nat. Commun.* **7**, 13108 (2016).
16. Krishna, G. R., Devarapalli, R., Lal, G. & Reddy, C. M. Mechanically flexible organic crystals achieved by introducing weak interactions in structure: supramolecular shape synthons. *J. Am. Chem. Soc.* **138**, 13561–13567 (2016).
17. Saha, S. & Desiraju, G. R. Acid•••amide supramolecular synthon in cocrystals: from spectroscopic detection to property engineering. *J. Am. Chem. Soc.* **140**, 6361–6373 (2018).
18. Ahmed, E., Karothu, D. P., Warren, M. & Naumov, P. Shape-memory effects in molecular crystals. *Nat. Commun.* **10**, 3723 (2019).
19. Commins, P., Al-Handawi, M. B., Karothu, D. P., Raj, G. & Naumov, P. Efficiently self-healing boronic ester crystals. *Chem. Sci.* **11**, 2606–2613 (2020).
20. Huang, R., Wang, C., Wang, Y. & Zhang, H. Elastic self-doping organic single crystals exhibiting flexible optical waveguide and amplified spontaneous emission. *Adv. Mater.* **30**, 1800814 (2018).
21. Panda, M. K. et al. Spatially resolved analysis of short-range structure perturbations in a plastically bent molecular crystal. *Nat. Chem.* **7**, 65–72 (2015).
22. Saha, S. & Desiraju, G. R. Crystal engineering of hand-twisted helical crystals. *J. Am. Chem. Soc.* **139**, 1975–1983 (2017).
23. Liu, H., Ye, K., Zhang, Z. & Zhang, H. An organic crystal with high elasticity at an ultra-low temperature (77 K) and shapeability at high temperatures. *Angew. Chem. Int. Ed.* **58**, 19081–19086 (2019).
24. Hayashi, S. & Koizumi, T. Elastic organic crystals of a fluorescent π-conjugated molecule. *Angew. Chem. Int. Ed.* **55**, 2701–2704 (2016).
25. Liu, H. et al. Controllably realizing elastic/plastic bending based on a room-temperature phosphorescent waveguiding organic crystal. *Chem. Sci.* **10**, 227–232 (2019).
26. Huang, R., Tang, B., Ye, K., Wang, C. & Zhang, H. Flexible luminescent organic bulk crystal: 2D elasticity toward 3D optical waveguide. *Adv. Optical Mater.* **7**, 1900927 (2019).
27. Lu, Z. et al. Optical waveguiding organic single crystals exhibiting physical and chemical bending features. *Angew. Chem. Int. Ed.* **59**, 4299–4303 (2020).
28. Zhao, W. et al. Boosting the efficiency of organic persistent room-temperature phosphorescence by intramolecular triplet-triplet energy transfer. *Nat. Commun.* **10**, 1595 (2019).
29. Wu, X. et al. Exploiting racemism enhanced organic room-temperature phosphorescence to demonstrate Wallach's rule in the lighting chiral chromophores. *Nat. Commun.* **11**, 2145 (2020).
30. Sun, M. et al. In situ visualization of assembly and photonic signal processing in a triplet light-harvesting nanosystem. *J. Am. Chem. Soc.* **140**, 4269–4278 (2018).
31. Zhao, W. et al. Rational molecular design for achieving persistent and efficient pure organic room-temperature phosphorescence. *Chem* **1**, 592–602 (2016).
32. Lee, D. R. et al. Heavy atom effect of selenium for metal-free phosphorescent light-emitting diodes. *Chem. Mater.* **32**, 2583–2592 (2020).
33. An, Z. et al. Stabilizing triplet excited states for ultralong organic phosphorescence. *Nat. Mater.* **14**, 685–690 (2015).
34. Mao, Z. et al. The methylation effect in prolonging the pure organic room temperature phosphorescence lifetime. *Chem. Sci.* **10**, 179–184 (2019).
35. Wang, X. et al. Pure organic room temperature phosphorescence from excited dimers in self-assembled nanoparticles under visible and near-infrared irradiation in water. *J. Am. Chem. Soc.* **141**, 5045–5050 (2019).
36. Wang, J. et al. Time-dependent afterglow color in a single-component organic molecular crystal. *Angew. Chem. Int. Ed.* **59**, 10032–10036 (2020).
37. Yang, C. et al. Controllable co-assembly of organic micro/nano heterostructures from fluorescent and phosphorescent molecules for dual anti-counterfeiting. *Mater. Horiz.* **6**, 984–989 (2019).
38. Bolton, O., Lee, K., Kim, H., Lin, K. Y. & Kim, J. Activating efficient phosphorescence from purely organic materials by crystal design. *Nat. Chem.* **3**, 205–210 (2011).
39. Li, D. et al. Amorphous metal-free room-temperature phosphorescent small molecules with multicolor photoluminescence via a host–guest and dual-emission strategy. *J. Am. Chem. Soc.* **140**, 1916–1923 (2018).
40. Han, J. et al. Small-molecule-doped organic crystals with long-persistent luminescence. *Adv. Funct. Mater.* **29**, 1902503 (2019).
41. Bian, L. et al. Simultaneously enhancing efficiency and lifetime of ultralong organic phosphorescence materials by molecular self-assembly. *J. Am. Chem. Soc.* **140**, 10734–10739 (2018).
42. Wang, J., Huang, Z., Ma, X. & Tian, H. Visible-light-excited room-temperature phosphorescence in water by cucurbit [8] uril-mediated supramolecular assembly. *Angew. Chem. Int. Ed.* **59**, 9928–9933 (2020).
43. Zhang, T., Ma, X. & Tian, H. A facile way to obtain near-infrared room-temperature phosphorescent soft materials based on bodipy dyes. *Chem. Sci.* **11**, 482–487 (2020).
44. Gu, M. et al. Polymorphism-dependent dynamic ultralong organic phosphorescence. *Research*. **2020**, 8183450 (2020).
45. Zhou, Q. et al. A clustering-triggered emission strategy for tunable multicolor persistent phosphorescence. *Chem. Sci.* **11**, 2926–2933 (2020).
46. Liu, B. et al. Red-emissive organic crystals of a single-benzene molecule: elastically bendable and flexible optical waveguide. *J. Phys. Chem. Lett.* **10**, 1437–1442 (2019).
47. Ghosh, S., Mishra, M. K., Kadambi, S. B., Ramamurty, U. & Desiraju, G. R. Designing elastic organic crystals: highlyflexible polyhalogenated n-benzylideneanilines. *Angew. Chem. Int. Ed.* **54**, 2674–2678 (2015).
48. Lin, Z., Kabe, R., Wang, K. & Adachi, C. Influence of energy gap between charge-transfer and locally excited states on organic long persistence luminescence. *Nat. Commun.* **11**, 191 (2020).

ACKNOWLEDGEMENTS

This work is supported by the National Natural Science Foundation of China (21875104, 21975120, 21973043, 91833304 61935017, and 51673095), Natural Science Fund for Distinguished Young Scholars of Jiangsu Province (BK20180037), Projects of International Cooperation and Exchanges NSFC (51811530018) and the

Fundamental Research Funds for the Central Universities. We are grateful to the High-Performance Computing Center of Nanjing Tech University for technical support. Kaiwei Huang and Lulu Song contributed equally to this work.

AUTHOR CONTRIBUTIONS

K.H. and L.S. contributed equally to this work. K.H., L.S., W.Y., Z.A. and W.H. conceived and designed the research. K.L., M.G., H.S. and M.S. polished the article. A.L. and H.M. provided theoretical calculations. J.S., J.W., H.W. and G.S. analyzed the mechanical bending characteristics of crystals. K.S., W.Y., Z.A. and W.H. provided useful advice throughout the research.

COMPETING INTERESTS

The authors declare no competing interests.

ADDITIONAL INFORMATION

Supplementary information The online version contains supplementary material available at https://doi.org/10.1038/s41528-021-00117-9.

Correspondence and requests for materials should be addressed to W.Y., Z.A. or W.H.

Reprints and permission information is available at http://www.nature.com/reprints

Publisher's note Springer Nature remains neutral with regard to jurisdictional claims in published maps and institutional affiliations.